A Foundation Model for Chest X-ray Interpretation with Grounded Reasoning via Online Reinforcement Learning

Qika Lin[1], Yifan Zhu[2], Bin Pu[3], Ling Huang[4], Haoran Luo[5], Jingying Ma[1], Zhen Peng[6], Tianzhe Zhao[6], Fangzhi Xu[6], Jian Zhang[6], Kai He[1], Zhonghong Ou[2], Swapnil Mishra[1], and Mengling Feng[1]

[1]National University of Singapore [2]Beijing University of Posts and Telecommunications
[3]The Hong Kong University of Science and Technology [4]Imperial College London
[5]Nanyang Technological University [6]Xi'an Jiaotong University
qikalin@foxmail.com, swapnil.mishra@nus.edu.sg, ephfm@nus.edu.sg

Abstract

Medical foundation models (FMs) have shown tremendous promise amid the rapid advancements in artificial intelligence (AI) technologies. However, current medical FMs typically generate answers in a black-box manner, lacking transparent reasoning processes and locally grounded interpretability, which hinders their practical clinical deployments. To this end, we introduce DeepMedix-R1, a holistic medical FM for chest X-ray (CXR) interpretation. It leverages a sequential training pipeline: initially fine-tuned on curated CXR instruction data to equip with fundamental CXR interpretation capabilities, then exposed to high-quality synthetic reasoning samples to enable cold-start reasoning, and finally refined via online reinforcement learning to enhance both grounded reasoning quality and generation performance. Thus, the model produces both an answer and reasoning steps tied to the image's local regions for each query. Quantitative evaluation demonstrates substantial improvements in report generation (e.g., 14.54% and 31.32% over LLaVA-Rad and MedGemma) and visual question answering (e.g., 57.75% and 23.06% over MedGemma and CheXagent) tasks. To facilitate robust assessment, we propose Report Arena, a benchmarking framework using advanced language models to evaluate answer quality, further highlighting the superiority of DeepMedix-R1. Expert review of generated reasoning steps reveals greater interpretability and clinical plausibility compared to the established Qwen2.5-VL-7B model (0.7416 vs. 0.2584 overall preference). Collectively, our work advances medical FM development toward holistic, transparent, and clinically actionable modeling for CXR interpretation.

1 Introduction

Recent years have witnessed remarkable progress in the development of generative artificial intelligence (AI), with foundation models (FMs) emerging as a unifying framework for integrating knowledge across domains. By pretraining on large-scale, heterogeneous datasets, FMs—including both large language models (LLMs) [1] and vision-language models (VLMs) [2]—have demonstrated the capacity to address a broad array of downstream tasks [3–6] through a single and adaptable architecture. This paradigm shift, in which a single FM serves as the foundation for diverse applications, has rapidly gained traction within the AI community [7, 8].

Preprint. Under review.

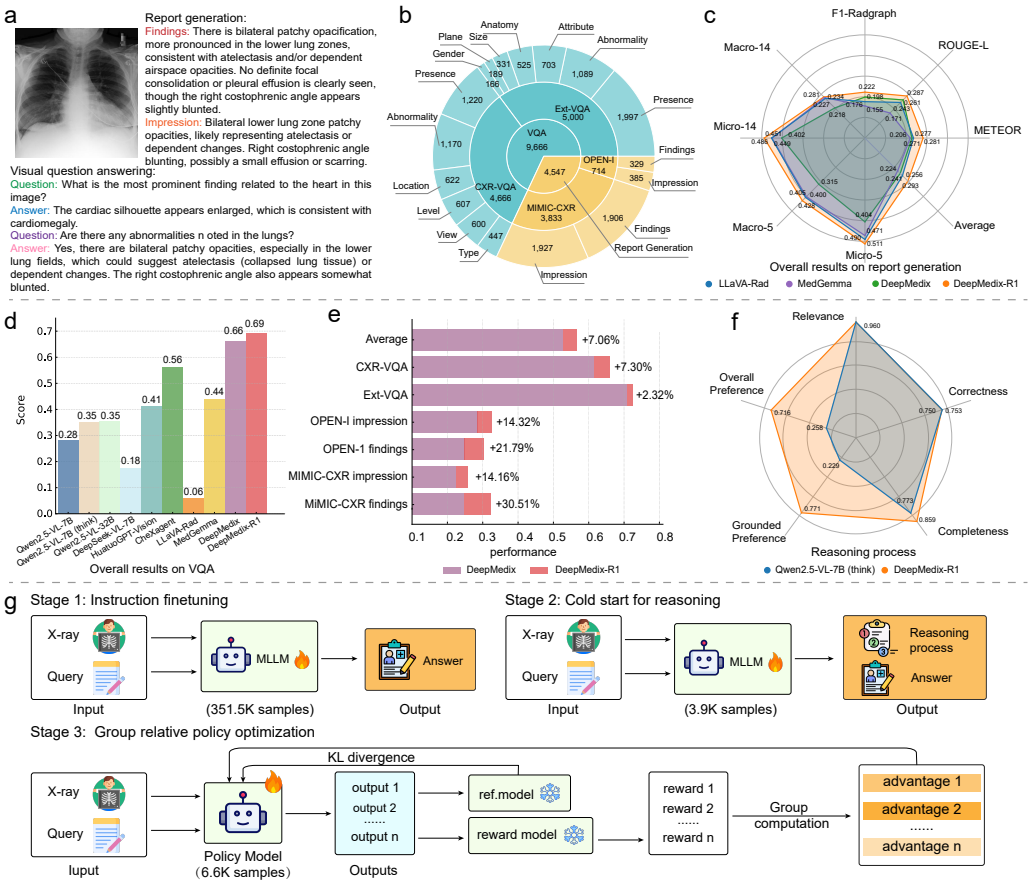

Figure 1: The overall architecture and experimental results of DeepMedix-R1. (a) is the illustration for the report generation and VQA tasks. (b) is the data distribution of the XrayBench for testing. (c) and (d) are the results for model comparison on report generation and VQA, respectively, demonstrating DeepMedix-R1 outperforms state-of-the-art open-source FMs in both general and medical domains. The metrics Micro-5, Macro-5, Micro-14, and Macro-14 are obtained from F1-CheXbert. (e) is the general comparison between DeepMedix and DeepMedix-R1. (f) is the expert annotation for reasoning processes from five dimensions. (g) is the illustration of the supervised fine-tuning and reinforcement learning stages.

Under this broader context, FMs in the medical domain have exhibited significant potential, garnering increasing attention from both academia and industry. These advanced AI systems, trained on vast multimodal datasets—including medical imaging, electronic health records, and biomedical literature—demonstrate transformative capabilities across diverse healthcare applications [9–12]. By processing and analyzing complex medical data at scale while adapting to specialized clinical tasks through fine-tuning, they emerge as powerful tools for improving diagnostic accuracy, optimizing workflows, and potentially accelerating medical discoveries [13]. For instance, Li et al. [14] introduce a comprehensive collection of biomedical multimodal instruction-following data and propose a curriculum learning strategy for their FM, LLaVA-Med. This vision-language conversational assistant is specifically designed to address open-ended research questions related to biomedical images. Similarly, Gao et al. [15] present ALPaCA, a slide-level FM for computational pathology, which achieves robust performance in whole-slide image question answering across multiple cancer types and tissue sites. Additionally, Zambrano et al. [16] develop LLaVA-Rad using a systematic three-phase approach involving pre-training, alignment, and fine-tuning. Their model outperforms both larger general-purpose models and domain-specific alternatives in chest X-ray report generation.

Despite their promise, current open-source medical FMs typically suffer from two critical limitations. First, the absence of transparent reasoning significantly hinders their clinical utility, as current models predominantly operate as black boxes and generate diagnostic outputs without revealing the

underlying clinical rationale [17]. This lack of interpretability prevents healthcare professionals from verifying that the model is making accurate decisions based on the facts of the disease—a major concern in high-stakes medical environments where explainability is paramount [18, 19]. Second, current models exhibit limited capability in precisely localizing individual findings within medical images [20–22]. Although these systems demonstrate proficiency in holistic image interpretation, they often fail to identify and analyze clinically relevant localized regions comprehensively. This constitutes a critical limitation since radiological and pathological diagnoses fundamentally rely on meticulous evaluation of specific anatomical features or pathological abnormalities at a granular level [23, 24]. Moreover, the evaluation of medical FMs presents a critical yet formidable challenge. Unlike conventional AI systems that produce structured outputs, medical FMs typically generate unstructured free-text responses (e.g., diagnostic reports), making automated assessment complicated. This challenge is compounded by the fact that divergent responses may represent clinically plausible variations rather than errors, necessitating expert evaluation with specialized medical knowledge. Consequently, this reliance on human expertise introduces inherent subjectivity and scalability limitations [25]. Conventional natural language generation (NLG) metrics (e.g., BLEU [26], METEOR [27], and ROUGE-L [28]) are fundamentally limited to assessing surface-level textual similarity and fail to capture clinical validity and nuance, highlighting the need for domain-specific evaluation frameworks.

To address these limitations, we propose a novel approach integrating grounded interpretation and step-wise reasoning for medical image analysis using FMs, with a specific focus on chest X-rays (CXRs). The overall architecture and experimental results are shown in Fig.1. First, we systematically curated a comprehensive multi-source CXR dataset encompassing diverse clinical scenarios, including report generation (*findings* and *impression* sections), visual question answering (VQA), and localized image interpretation. Building upon this foundation, we adapted the state-of-the-art general-purpose VLM Qwen2.5-VL-7B [29] through extensive instruction fine-tuning (351.5K samples), equipping the resulting DeepMedix model with fundamental CXR interpretation capabilities. Second, we generated high-quality synthetic reasoning data (3.9K samples) incorporating grounded image representations to overcome the model cold-start problems [30, 31]. The continuous fine-tuning upon it endows the model with preliminary capabilities in grounded understanding and reasoning. Finally, we implemented an advanced online reinforcement learning framework, i.e., group relative policy optimization (GRPO) [30], to simultaneously enhance both reasoning quality and generation performance of DeepMedix by scoring both the final outputs and the underlying reasoning processes. This scoring mechanism serves as feedback to iteratively optimize the model (on 6.6K samples), ultimately creating our enhanced DeepMedix-R1 model.

To comprehensively evaluate the CXR interpretation capabilities of open-source FMs across both general and medical-specific domains, we developed XrayBench (as shown in Fig.1b), a multimodal evaluation framework comprising 14.2K carefully curated samples. This benchmark systematically assesses model performance on two clinically critical tasks: report generation (including both findings and impression sections), and VQA, utilizing data from four diverse medical imaging datasets. To assess the quality of the final output, conventional NLG-based metrics and fact-based evaluation are utilized. Besides, an LLM-as-judge evaluation framework for comprehensive performance analysis, namely Report Arena, is introduced to assess paired outputs from competing models on report generation tasks. Additionally, CXR experts conduct a comprehensive evaluation of the reasoning process. We have three key observations from the experiment results: (1) On automated metrics for both report generation (NLG-based metrics like BLEU, METEOR and ROUGE-L, and fact-based metrics like F1-RadGraph [32] and F1-CheXbert [33]) and VQA (accuracy), DeepMedix-R1 outperforms state-of-the-art open-source FMs in both general and medical domains, achieving 31.32% and 57.75% higher than MedGemma [34] on report generation and VQA tasks, respectively; (2) We implement an LLM-as-judge evaluation framework (i.e., Report Arena) to comparatively assess paired outputs from competing models on report generation tasks. This approach, analogous to Chatbot Arena's methodology [35], enables systematic quality ranking through LLM-mediated pairwise comparisons; Benchmarking results position DeepMedix-R1 in first place, followed sequentially by LLaVA-Rad [16], DeepMedix, and MedGemma models. (3) We carry out annotation by four domain experts who evaluate the reasoning processing across five key dimensions, i.e., *Relevance*, *Correctness*, *Completeness*, *Grounded Preference*, and *Overall Preference*. Evaluation results demonstrate that DeepMedix-R1 generally outperforms Qwen2.5-VL-7B in reasoning quality and is strongly preferred by medical experts.

2 Results

Overview of Results

In the experiment, we employ three general-purpose vision-language FMs: Qwen2.5-VL-7B [29], Qwen2.5-VL-32B [29], DeepSeek-VL-7B [36]. To investigate the effects of grounded understanding and reasoning, we introduce Qwen2.5-VL-7B (think) that employs specialized prompting to enable the Qwen2.5-VL-7B model to generate both the reasoning process and the final answer simultaneously. For comparative analysis, we additionally evaluate two medical FMs (HuatuoGPT-Vision [37] and MedGemma [34]) and two CXR-specific FMs (CheXagent [38] and LLaVA-Rad [16]). The XrayBench for testing integrates four key datasets: two for report generation (MIMIC-CXR [39] and Open-I [40]) and two for VQA (Ext-VQA [41] and CXR-VQA [42]). Its detailed statistics are shown in Fig.1b.

The overall results for report generation and VQA of DeepMedix-R1 and baselines are shown in Fig.1c and Fig.1d, respectively. For report generation, DeepMedix-R1 outperforms all compared models—including the supervised fine-tuning baseline DeepMedix, as well as state-of-the-art domain-specific models LLaVA-Rad and MedGemma—across all evaluation metrics, with average improvements of 21.76%, 14.54%, and 31.32%, respectively. For VQA, DeepMedix-R1 also performs best across all baselines, while LLaVA-Rad shows a relatively limited performance as it is specifically fine-tuned only for report generation tasks. Compared with strong baselines like DeepMedix, MedGemma, and CheXagent, DeepMedix-R1 has an improvement of 4.54%, 57.75%, and 23.06%, respectively. We also show the effectiveness of the online reinforcement learning in Fig.1e. DeepMedix-R1 demonstrates an average improvement of 7.06% over DeepMedix, with significant gains across all benchmarks: 30.51% on MIMIC-CXR findings, 14.16% on MIMIC-CXR impression, 21.79% on OPEN-I findings, 14.32% on OPEN-I impression, 2.32% on Ext-VQA, and 7.30% on CXR-VQA. These results highlight the substantial positive impact of integrating online reinforcement learning into CXR FMs. We provide detailed analyses in subsequent sections.

Automated metrics on report generation

At the beginning, to have an overview of the model generation, we provide length distributions for ground truth and results from LLaVA-Rad, DeepMedix, and DeepMedix-R1, on MIMIC-CXR findings, MIMIC-CXR impression, OPEN-I findings, and MIMIC-CXR impression. The results are shown in Fig.2abcd, respectively. From them, we find that after the first stage, DeepMedix and LLaVA-Rad demonstrate comparable results to the ground truth in terms of report length alignment. LLaVA-Rad wound generate more tokens on MIMIC-CXR impression and OPEN-I findings than ground truth, which could potentially produce unnecessary or incorrect information. After online reinforcement learning, the distribution of model DeepMedix-R1 demonstrates a more pronounced shift toward the desired direction to truth on MIMIC-CXR findings and OPEN-I impression, compared with DeepMedix. On MIMIC-CXR impression and OPEN-I findings, DeepMedix-R1 would generate more tokens and be more inclined to generate responses of average length (i.e., 40–60).

The detailed results of the report generation are summarized in Tab.1 and the average performance across four tasks is shown in Fig.2e. For the detailed components of the test sets, i.e., MIMIC-CXR findings, MIMIC-CXR impression, OPEN-I findings, and OPEN-I impression, it is evident that general-purpose models perform poorly across both NLG-based and fact-based evaluation metrics. Among FMs in the medical domain, LLaVA-Rad serves as a strong baseline, particularly on the MIMIC-CXR findings and MIMIC-CXR impression sections. However, our proposed DeepMedix-R1 achieves an average improvement of 10.20% (0.3230 vs. 0.2931) and 10.47% (0.2563 vs. 0.2320), respectively. On average, we can observe that DeepMedix-R1 consistently outperforms all other models, achieving the highest scores in most metrics and the overall highest weighted average of 0.2934. Specifically, the general-purpose FMs (Qwen2.5-VL-7B, Qwen2.5-VL-32B, and DeepSeek-VL-7B) exhibit limited performance. The best model Qwen2.5-VL-32B among them has an average of 0.1433, which is only 28.84% of DeepMedix-R1. Also, the thinking process does not enhance the model's performance. Compared with medical FMs, DeepMedix-R1 has obvious improvements, i.e., 69.63% for HuatuoGPT-Vision (0.1730), 75.30% for CheXagent (0.1674), 14.54% for LLaVA-Rad (0.2562), 31.20% for MedGemma (0.2236). Furthermore, compared with fine-tuned DeepMedix, DeepMedix-R1 demonstrates consistent improvements across all four test components as well as the

Table 1: The report generation results are presented for MIMIC-CXR findings, MIMIC-CXR impression, OPEN-I findings, and MIMIC-CXR impression, followed by the weighted average across these four splits. The metrics Micro-5, Macro-5, Micro-14, and Macro-14 are obtained from F1-CheXbert. The best and second-best values for each metric are highlighted in bold and boxed, respectively.

Model	NLG-based Metric						Fact-based Metric					Average
	BLEU-1	BLEU-2	BLEU-3	BLEU-4	METEOR	ROUGE-L	F1-RadGraph	Macro-14	Micro-14	Macro-5	Micro-5	
MIMIC-CXR Findings												
Qwen2.5-VL-7B	0.0732	0.0367	0.0200	0.0117	0.1932	0.1434	0.0930	0.1327	0.2137	0.1643	0.1769	0.1144
Qwen2.5-VL-7B (think)	0.0615	0.0304	0.0197	0.0147	0.0764	0.1106	0.0493	0.1198	0.1741	0.1492	0.1509	0.0870
Qwen2.5-VL-32B	0.0887	0.0440	0.0235	0.0136	0.2127	0.1538	0.0921	0.2260	0.3461	0.3258	0.3476	0.1704
DeepSeek-VL-7B	0.1356	0.0566	0.0300	0.0194	0.1673	0.1730	0.0619	0.1300	0.2444	0.1118	0.1710	0.1183
HuatuoGPT-Vision	0.2244	0.1133	0.0631	0.0390	0.2361	0.1998	0.1127	0.2222	0.3532	0.3543	0.4099	0.2116
CheXagent	0.0277	0.0170	0.0134	0.0115	0.0424	0.0658	0.0965	0.1275	0.1818	0.1935	0.2479	0.0932
LLaVA-Rad	0.2911	0.1757	0.1189	0.0846	0.2500	0.2928	0.2077	**0.3154**	0.4753	0.4592	0.5535	0.2931
MedGemma	0.1752	0.0960	0.0586	0.0377	0.2613	0.2122	0.1864	0.3347	0.5041	0.4616	0.5183	0.2587
DeepMedix	0.2445	0.1589	0.1147	0.0871	0.2291	0.2870	0.1832	0.2271	0.3956	0.3476	0.4477	0.2475
DeepMedix-R1	**0.3402**	**0.2149**	**0.1479**	**0.1059**	**0.2895**	**0.3292**	**0.2387**	0.3126	**0.5189**	**0.4821**	**0.5726**	**0.3230**
MIMIC-CXR Impression												
Qwen2.5-VL-7B	0.0616	0.0280	0.0164	0.0112	0.1323	0.0975	0.0710	0.2072	0.3053	0.3258	0.3635	0.1473
Qwen2.5-VL-7B (think)	0.0628	0.0414	0.0347	0.0311	0.0720	0.0836	0.0475	0.1475	0.2199	0.2088	0.2352	0.1077
Qwen2.5-VL-32B	0.0624	0.0279	0.0164	0.0113	0.1392	0.0939	0.0585	0.2028	0.3117	0.3190	0.3454	0.1444
DeepSeek-VL-7B	0.0624	0.0272	0.0171	0.0126	0.1026	0.0942	0.0273	0.1386	0.2245	0.1288	0.1634	0.0908
HuatuoGPT-Vision	0.1176	0.0556	0.0342	0.0243	0.1651	0.1225	0.0714	0.1959	0.3227	0.3347	0.3874	0.1665
CheXagent	0.1795	0.1337	0.1140	0.1033	0.2032	0.2162	**0.1792**	0.2359	0.4130	0.3866	0.4417	0.2369
LLaVA-Rad	0.1852	0.1074	0.0741	0.0546	0.2135	0.1961	0.1396	0.2498	0.4258	0.4195	0.4865	0.2320
MedGemma	0.1321	0.0699	0.0480	0.0361	0.1759	0.1368	0.1177	0.2465	0.4146	0.4199	0.4861	0.2076
DeepMedix	0.1682	**0.1378**	**0.1231**	**0.1151**	0.1884	0.2089	0.1779	0.2100	0.3744	0.3346	0.4314	0.2245
DeepMedix-R1	**0.2135**	0.1376	0.1035	0.0832	**0.2379**	**0.2191**	0.1739	**0.2697**	**0.4491**	**0.4249**	**0.5071**	**0.2563**
OPEN-I Findings												
Qwen2.5-VL-7B	0.0468	0.0263	0.0165	0.0104	0.1706	0.1298	0.1344	0.0576	0.1302	0.0264	0.0280	0.0706
Qwen2.5-VL-7B (think)	0.0984	0.0575	0.0418	0.0336	0.1000	0.1418	0.0939	0.0729	0.3281	0.0372	0.0451	0.0955
Qwen2.5-VL-32B	0.0577	0.0310	0.0188	0.0118	0.1925	0.1384	0.1083	0.0693	0.1093	0.0631	0.0800	0.0800
DeepSeek-VL-7B	0.0822	0.0369	0.0224	0.0154	0.1680	0.1575	0.1366	0.0816	0.2331	0.0573	0.1111	0.1002
HuatuoGPT-Vision	0.0883	0.0464	0.0284	0.0184	0.2298	0.1610	0.1483	0.1019	0.1853	0.1524	0.2093	0.1245
CheXagent	0.0560	0.0376	0.0287	0.0236	0.0643	0.0758	0.0655	0.1364	0.2349	0.1709	0.2750	0.1062
LLaVA-Rad	0.3397	0.2150	0.1469	0.1106	0.3032	0.3464	0.2859	0.2131	0.3790	0.2600	0.3211	0.2655
MedGemma	0.1530	0.0955	0.0643	0.0442	0.2909	0.2150	0.2874	0.2195	0.3756	0.1621	0.3143	0.2020
DeepMedix	0.3298	0.2098	0.1556	0.1215	0.2916	0.3384	0.2907	0.1631	0.3852	0.1943	0.2453	0.2478
DeepMedix-R1	**0.3958**	**0.2535**	**0.1834**	**0.1362**	**0.3846**	**0.3753**	**0.3267**	**0.2498**	**0.3905**	**0.2952**	**0.3286**	**0.3018**
OPEN-I Impression												
Qwen2.5-VL-7B	0.0280	0.0155	0.0111	0.0085	0.0943	0.0590	0.0415	0.1005	0.1826	0.1089	0.1385	0.0717
Qwen2.5-VL-7B (think)	0.0556	0.0451	0.0414	0.0396	0.0641	0.0614	0.0321	0.0685	0.2162	0.0514	0.0752	0.0682
Qwen2.5-VL-32B	0.0276	0.0147	0.0105	0.0080	0.1002	0.0546	0.0418	0.0790	0.1031	0.0947	0.1044	0.0581
DeepSeek-VL-7B	0.0553	0.0289	0.0228	0.0195	0.1117	0.0761	0.0293	0.0910	0.4715	0.0380	0.0561	0.0909
HuatuoGPT-Vision	0.0224	0.0111	0.0080	0.0062	0.0781	0.0491	0.0272	0.0751	0.0949	0.1065	0.1296	0.0553
CheXagent	0.2544	0.2136	0.1919	0.1764	0.2470	0.2542	0.1815	0.1935	0.5775	0.1521	0.1831	0.2387
LLaVA-Rad	0.1442	0.0854	0.0647	0.0532	0.2027	0.1450	0.1061	0.2019	0.5172	0.1923	0.3333	0.1860
MedGemma	0.0863	0.0533	0.0411	0.0339	0.1566	0.1003	0.0732	0.1910	0.4086	0.1999	0.2887	0.1484
DeepMedix	**0.3639**	0.2820	0.2332	0.2305	0.3565	0.3224	**0.2909**	0.1162	0.5847	0.1633	0.1913	0.2850
DeepMedix-R1	0.3426	**0.2888**	**0.2577**	**0.2377**	**0.3628**	**0.3457**	**0.2893**	**0.2061**	**0.5915**	**0.2837**	**0.3774**	**0.3258**
Weighted Average												
Qwen2.5-VL-7B	0.0625	0.0305	0.0175	0.0111	0.1574	0.1158	0.0823	0.1561	0.2438	0.2181	0.2420	0.1216
Qwen2.5-VL-7B (think)	0.0642	0.0383	0.0295	0.0251	0.0752	0.0972	0.0503	0.1238	0.2082	0.1581	0.1726	0.0948
Qwen2.5-VL-32B	0.0701	0.0338	0.0191	0.0120	0.1706	0.1189	0.0748	0.1924	0.2938	0.2843	0.3067	0.1433
DeepSeek-VL-7B	0.0939	0.0404	0.0234	0.0162	0.1352	0.1303	0.0499	0.1268	0.2544	0.1088	0.1537	0.1030
HuatuoGPT-Vision	0.1522	0.0754	0.0437	0.0285	0.1922	0.1515	0.0905	0.1899	0.3063	0.3104	0.3621	0.1730
CheXagent	0.1133	0.0846	0.0723	0.0652	0.1295	0.1462	0.1365	0.1797	0.3171	0.2702	0.3265	0.1674
LLaVA-Rad	0.2373	0.1420	0.0974	0.0711	0.2344	0.2432	0.1759	0.2706	0.4509	0.4054	0.4896	0.2562
MedGemma	0.1478	0.0813	0.0530	0.0372	0.2184	0.1710	0.1550	0.2768	0.4488	0.4001	0.4705	0.2236
DeepMedix	0.2284	0.1641	0.1313	**0.1136**	0.2272	0.2606	0.1979	0.2058	0.4019	0.3154	0.4044	0.2410
DeepMedix-R1	**0.2907**	**0.1912**	**0.1409**	0.1096	**0.2807**	**0.2873**	**0.2219**	**0.2809**	**0.4862**	**0.4275**	**0.5107**	**0.2934**

average part (0.2934 vs. 0.2401), underscoring the efficacy of reinforcement learning in CXR report generation.

For detailed evaluation, we provide the CheXbert F1 score for top-10 supported medical observations in the report collection, as shown in Fig.2fg on MIMIC-CXR findings and OPEN-I findings, respectively. DeepMedix-R1 shows better F1 scores against baselines. On average across MIMIC-CXR findings, DeepMedix-R1 achieves a score of 0.4966, demonstrating significant improvements over existing FMs. Specifically, it outperforms Qwen2.5-VL-7B (0.2094) by 137.15%, HuatuoGPT-Vision (0.3050) by 62.80%, CheXagent (0.1788) by 177.75%, LLaVA-Rad (0.4562) by 8.86%, MedGemma (0.4487) by 10.69%, and even our baseline model (DeepMedix, 0.4176) by 18.91%. Across all observations, DeepMedix-R1 demonstrates optimal performance in detecting "Support Devices", "Pleural Effusion", "Lung Opacity", "Atelectasis", "Enlarged Cardiomediastinum", "Edema", and "No Finding" observations. However, its capability is relatively limited for "Cardiomegaly", "Pneumonia", and "Consolidation". On average across OPEN-I findings, DeepMedix-R1 achieves an F1 score of 0.3523, showing performance gains of 133.23% over Qwen2.5-VL-7B (0.1511), 83.10% over HuatuoGPT-

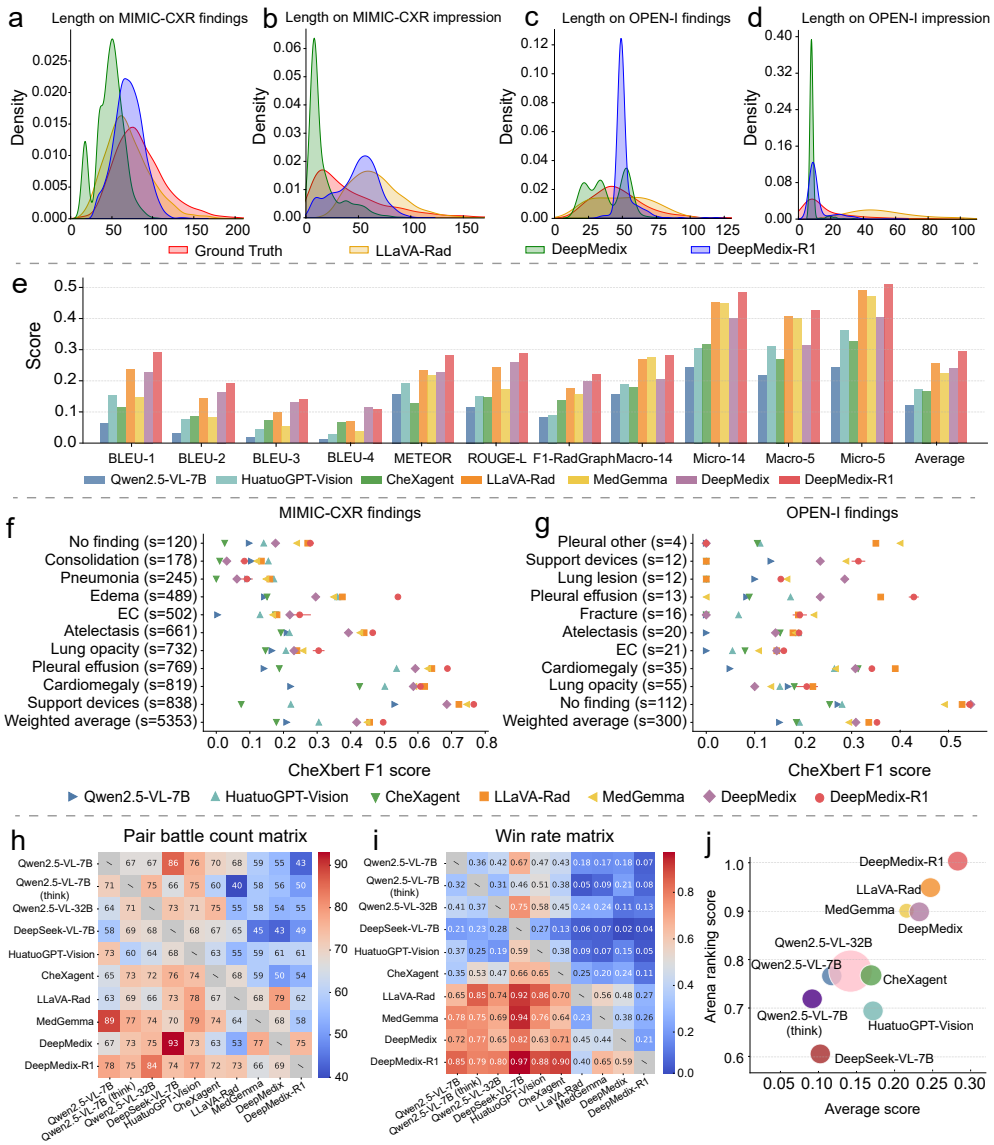

Figure 2: The results of the report generation tasks. (a), (b), (c), and (d) are the length distributions of the generated report in MIMIC-CXR findings, MIMIC-CXR impression, OPEN-I findings, and OPEN-I impression, respectively. (e) is the weighted average performance comparison across all report generation tasks. (f) and (g) are the detailed CheXbert-F1 scores on top-10 supported observations on MIMIC-CXR findings and OPEN-I findings, respectively. "EC" is short for "Enlarged Cardiomediastinum". (h) and (i) present the numerical matrices for pairwise model comparisons and corresponding win rates in our Report Arena evaluation framework, respectively. (j) comparatively visualizes each model's performance across both conventional automated metrics and Report Arena rankings, with circle sizes proportionally representing the number of model parameters.

Vision (0.1924), 89.52% over CheXagent (0.1859), 5.03% over LLaVA-Rad (0.3354), 19.71% over MedGemma (0.2943), 14.09% over DeepMedix (0.3088). Across all observations, DeepMedix-R1 demonstrates optimal performance for "No Finding" (comparable with DeepMedix), "Enlarged Cardiomediastinum", "Atelectasis", "Pleural Effusion", and "Support Devices". It achieves secondary performance levels for "Lung Opacity", "Cardiomegaly", "Fracture", and not good enough on "Lung Lesion", and "Pleural Other". Notably, while DeepMedix initially fails to outperform CheXagent and MedGemma models, the implementation of online reinforcement learning in DeepMedix-R1 yields substantial performance gains, ultimately surpassing all benchmark models.

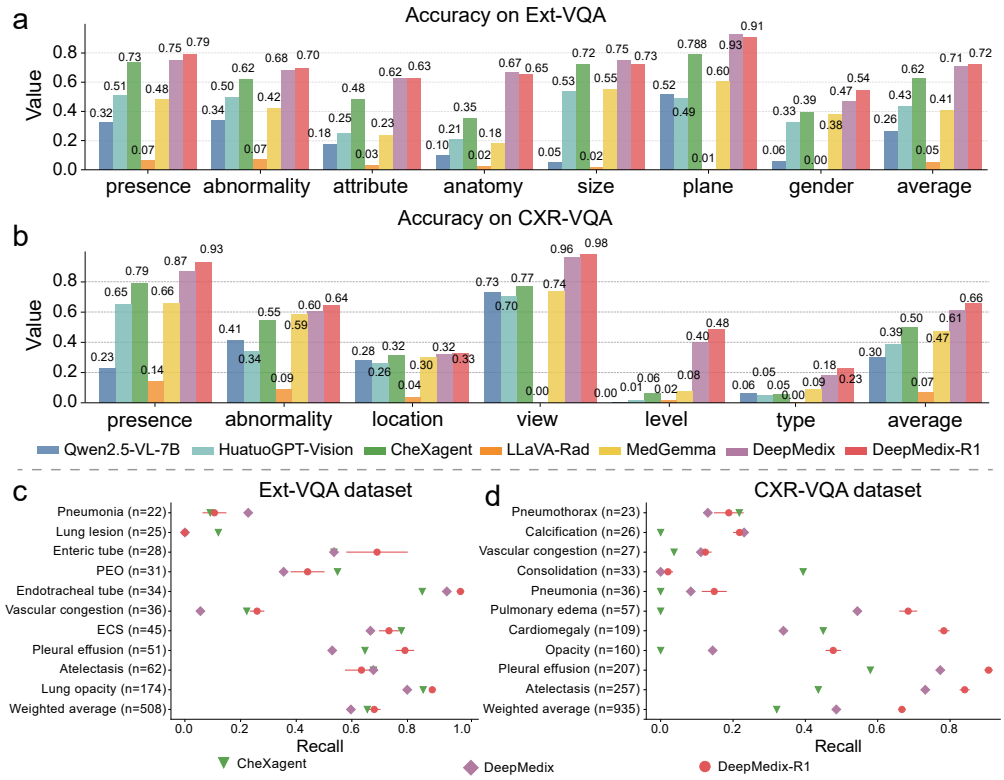

Figure 3: The results of the VQA tasks, demonstrating that our DeepMedix-R1 consistently outperforms competing models from both general and fine-grained perspectives. (a) and (b) are the accuracies across all different question types on Ext-VQA and CXR-VQA, respectively. (c) and (d) are the detailed F1 scores on top-10 observations on Ext-VQA and CXR-VQA, respectively. "PEO" is short for "Pulmonary edema/hazy opacity", and "ECS" is short for "Enlarged cardiac silhouette".

Results of Report Arena

Fig.2hij presents the pair battle count matrix, win rate matrix, and ranking scores from the report arena, respectively. ganjueFrom Fig.2i, models specifically designed for medical or CXR tasks (LLaVA-Rad, MedGemma, DeepMedix, and DeepMedix-R1) consistently outperform general-purpose vision-language models (e.g., Qwen2.5-VL-7B, Qwen2.5-VL-32B, and DeepSeek-VL-7B) across most comparisons. For example, DeepMedix achieves the 0.77 win rates against Qwen2.5-VL-7B (think) and 0.82 against DeepSeek-VL-7B. HuatuoGPT-Vision does not perform well compared with other baselines, failing to outperform even general-purpose models and only having a marginal advantage over DeepSeek-VL-7B with a win rate of 0.59. DeepMedix can win most baselines, except for LLaVA-Rad (win rate 0.45) and MedGemma (win rate 0.44). Further, DeepMedix-R1 can almost win all models, e.g., HuatuoGPT-Vision (0.88), CheXagent (0.90), MedGemma (0.65). While the (DeepMedix-R1, LLaVA-Rad) pair achieves a win rate of 0.4, the reverse pairing (LLaVA-Rad, DeepMedix-R1) shows a lower win rate of 0.27. From Fig.2j, it is observed that DeepMedix-R1 ranks first, followed by LLaVA-Rad, DeepMedix, MedGemma, Qwen2.5-VL-32B, CheXagent, Qwen2.5-VL-7B, Qwen2.5-VL-7B (think), HuatuoGPT-Vision, and DeepSeek-VL-7B in sequential order. The results demonstrate that larger model size improves performance, while the reasoning mode of general-purpose models fails to yield significant gains. Furthermore, we observe a moderately positive correlation between automated evaluation scores and ranking scores, with DeepMedix-R1 achieving top performance across both metric types.

Evaluation on VQA

The detailed results of the VQA are presented in Fig.3ab. As shown in the results, general-purpose models exhibit suboptimal performance in this domain. On the Ext-VQA dataset, DeepMedix-R1

Table 2: Expert annotation (two groups) result across five dimensions, i.e., relevance, correctness, completeness, grounded preference, and overall preference. The *agreement* illustrates inter-group labeling consistency, representing the agreement level among different annotation groups for the specified metric.

Model		Relevance	Correctness	Completeness	Grounded Preference	Overall Preference
Qwen2.5-VL-7B (think)	Group 1	0.9308	0.7622	0.6220	0.1905	0.2619
	Group 2	0.9899	0.7441	0.9238	0.2679	0.2548
	Average	0.9603	0.7531	0.7729	0.2292	0.2584
DeepMedix-R1	Group 1	0.9317	0.7014	0.7647	0.8095	0.7381
	Group 2	0.9886	0.7993	0.9536	0.7321	0.7452
	Average	0.9601	0.7503	0.8592	0.7708	0.7416
Agreement		0.9190	0.7686	0.7447	0.7762	0.7101

demonstrates superior accuracy across multiple question types, including presence, abnormality, attribute, anatomy, size, plane, and gender. Notably, DeepMedix achieves particularly competitive results in anatomy, size, and plane-related questions (e.g., 0.9101 accuracy for plane questions). On average, DeepMedix-R1 delivers significant performance improvements over state-of-the-art medical FMs, e.g., 66.97% over HuatuoGPT-Vision (0.4338), 16.04% over CheXagent (0.6242), 77.79% over MedGemma (0.4074). Similarly, on the CXR-VQA dataset, DeepMedix-R1 attains the highest accuracy across all question categories (presence, abnormality, location, view, level, and type). For instance, it achieves an accuracy of 0.9800 on "view" questions. Compared to leading medical FMs, DeepMedix-R1 shows substantial gains, e.g., 69.75% over HuatuoGPT-Vision (0.3881), 32.52% over CheXagent (0.4972), 39.27% over MedGemma (0.4731). In general, reinforcement learning enhances VQA performance, as evidenced by improved scores on both datasets (0.7243 vs. 0.7079 and 0.6589 vs. 0.6141, respectively).

We also compute recall rates for key abnormalities, attributes, and anatomical structures, with the top-10 highest-frequency objects visualized in Fig.3cd. On average of Ext-VQA dataset, our reasoning model DeepMedix-R1 achieves an average recall of 0.6804, demonstrating significant improvements over medical FMs, e.g., 3.80% over CheXagent (0.6555) and 14.07% over DeepMedix (0.5965). Notably, DeepMedix-R1 performs best on the following objects: "Lung opacity", "Pleural effusion", "Vascular congestion", "Endotracheal tube", and "Enteric tube". On average of CXR-VQA dataset, the performance gains are even more pronounced. Compared to medical FMs, DeepMedix-R1 achieves an average recall of 0.6670, with improvements of 107.85% over CheXagent (0.3209) and 37.36% over DeepMedix (0.4856). For nearly all objects—including "Atelectasis", "Pleural effusion", "Opacity", "Cardiomegaly", "Pulmonary edema", "Pneumonia", "Consolidation", and "Vascular congestion"—our method DeepMedix-R1 delivers the highest performance. The sole exception is "Pneumothorax", where it does not outperform alternatives. Additionally, our reasoning DeepMedix-R1 exhibits consistent improvements over DeepMedix across both datasets.

Expert evaluation for reasoning process

We present two concrete case studies in Fig.4 for findings generation and VQA, respectively, with all five annotation dimensions clearly illustrated. The final annotation of the reasoning process is shown in Tab.2. The agreement of the two groups is relatively high, with the highest 0.9190 at relevance and the lowest 0.7101 at overall preference. Qwen2.5-VL-7B (think) and DeepMedix-R1 perform comparably and are high at *Relevance* (0.9603 vs. 0.9601) but less at *Correctness* (0.7531 vs. 0.7503), indicating FMs usually generate relevant steps towards the answer while there is a large room for completely correct expression, regarded as a widespread hallucination problem in generative models [43]. The *Completeness* of Qwen2.5-VL-7B (think) is much less than DeepMedix-R1 (0.7729 vs. 0.8592), demonstrating Qwen2.5-VL-7B (think) model would miss some key reasoning steps. For model preference, DeepMedix-R1 scores higher than Qwen2.5-VL-7B (think) at both grounded and overall parts (0.7708 vs. 0.2292, 0.7416 vs. 0.2584), indicating our model is more likely to be accepted by professional doctors.

3 Discussion

To enhance the performance, reasoning ability, and grounded perception of FMs for CXRs, we introduce the DeepMedix-R1 model by instruction fine-tuning, cold start for reasoning, and group

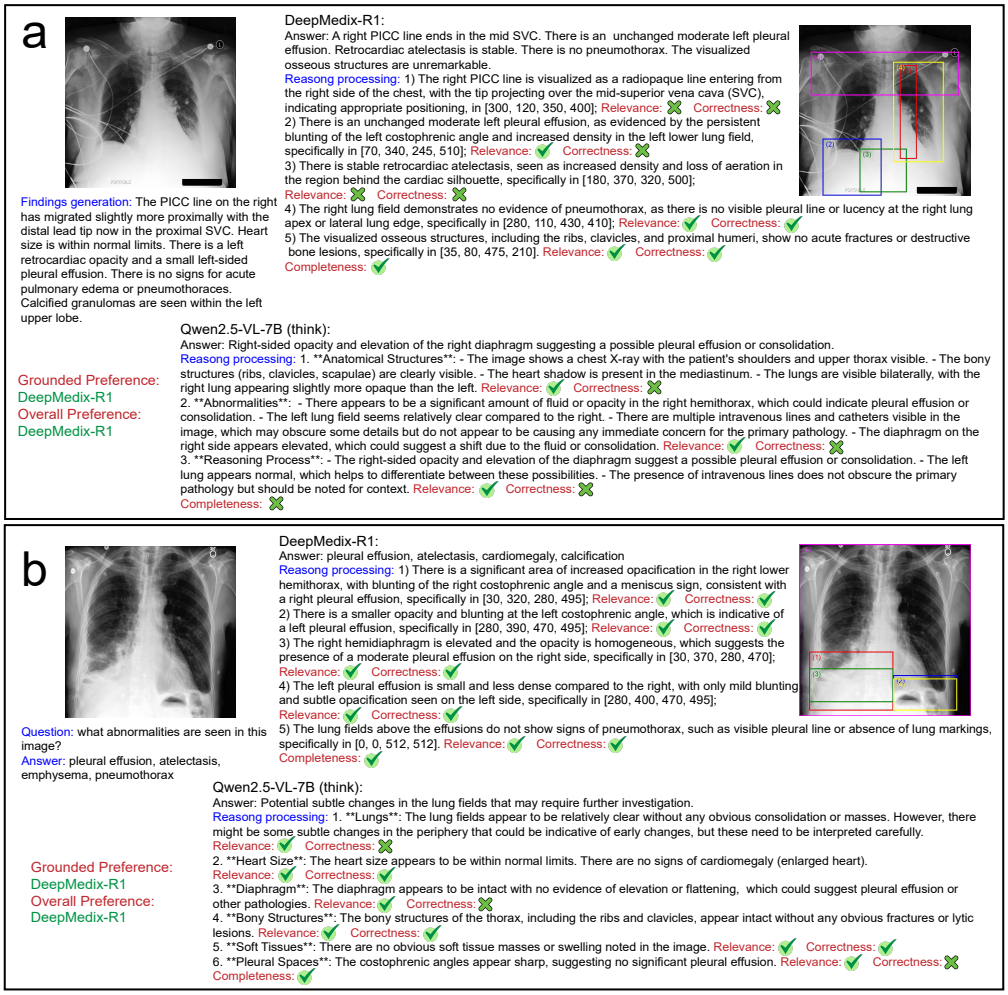

Figure 4: Two case studies for reasoning processing annotation across five dimensions, i.e., *Relevance*, *Correctness*, *Completeness*, *Grounded Preference*, and *Overall Preference*. It is observed that DeepMedix-R1 demonstrates superior performance in both grounded preference and overall preference for the reasoning process.

relative policy optimization stages. A comprehensive evaluation demonstrates that DeepMedix-R1 outperforms state-of-the-art open-source FMs in both general and medical-specific domains. Furthermore, online reinforcement learning significantly improves both model performance and reasoning capabilities.

Based on the results, we have three ways to the future work. Firstly, as online reinforcement learning is particularly beneficial for medical FMs, it enables them to continuously adapt and improve their performance based on real-time interactions and feedback. As there is a wealth of domain knowledge in the medical field [44, 45], it can be effectively leveraged to design a well-informed reward function for reinforcement learning. By incorporating expert insights, structured rules, or heuristic-based metrics into the reward mechanism, the reinforcement learning agent can receive more meaningful and interpretable feedback, guiding its learning process toward desired behaviors. This approach not only accelerates convergence by reducing sparse reward challenges but also enhances the model's alignment with domain-specific objectives, ensuring that the learned policies are both practical and high-performing in real-world applications.

Secondly, compared to general-purpose FMs designed for broad tasks, medical FMs tailored for healthcare applications still exhibit suboptimal performance in clinical settings. To address this limitation, strategies such as building larger and more finely curated datasets, diversifying task-specific training objectives, and aggregating biased data from multiple institutions and hospitals can

help mitigate performance gaps [46–48]. By incorporating more comprehensive and representative data, along with targeted task design, medical FMs can achieve improved accuracy, robustness, and generalizability in real-world clinical scenarios. It can be seen that our model indeed enhances the reasoning capability by utilizing the LLM-synthesized reasoning data and online reinforcement learning. However, it still suffers from the limitation of data quality. Thus, while acquiring latent medical reasoning process data is highly resource-intensive, it remains indispensable for training explainable FMs. A unified standard is also needed to make FMs easy to learn.

Finally, the annotation results indicate that the model achieves a *Correctness* score of 0.7503 and a *Completeness* score of 0.8592. While these metrics are significantly higher than baseline Qwen2.5-VL-7B (think), they remain insufficient for real-world deployment due to the persistent issue of hallucination in current FMs [49, 50]. Even minor inaccuracies or omissions would lead to critical errors in high-stakes applications in medical and healthcare domains. To mitigate this limitation, a substantial number of samples for the grounded understanding task can be incorporated during the fine-tuning phase. Also, in the future, further advancements in training methodologies—such as reinforcement learning with human feedback, adversarial validation, or hybrid neuro-symbolic approaches—will be essential to mitigate hallucinations and push correctness and completeness closer to the near-perfect levels required for reliable and scalable AI solutions.

4 Methods

Model Optimization

Like the LLM fine-tuning, in the first stage for instruction fine-tuning and the second stage for cold start reasoning, the next token prediction [51] is carried out to optimize FMs based on the instruction $\mathcal{Q}$ and X-ray $\mathcal{I}$ and previously generated text tokens with the loss function:

$$\mathcal{L}_{\mathrm{SFT}} = -\sum_{n=1}^{N} \log\left(x_n | x_{<n}, \mathcal{I}, \mathcal{O}\right). \tag{1}$$

In the second stage, we prompt closed-scoured GPT-4.1[1] to generate reasoning processing given X-rays, task prompt, and ground truth. We then check the validity of the derived reasoning procedures by prompting Qwen2.5-VL-32B and filter out those that are clearly unreasonable, e.g., the provided bounding box of the image region exceeds the maximum edge of the image. Finally, 3.9K samples are kept and used for the cold start training.

In the third stage, the GRPO algorithm [30] is utilized for online reinforcement learning to enhance the reasoning ability. Specifically, we optimize the model by comparing the relative performance of different policies or actions within the same group for CXR tasks, rather than relying on traditional critic models to evaluate the value of each action. It is to enable the model to compare its output with multiple candidate outputs generated by itself. Formally, $P(Q)$ denote the question set used for training. $q = [\mathcal{Q}, \mathcal{I}]$ is a sampled query in the current iteration. $\pi_{\theta_{\mathrm{old}}}$ and $\pi_{\theta_{\mathrm{new}}}$ (π_θ) denote the old policy and current new policy, respectively. o is a complete response sampled from a policy. Let $\pi_{\theta_{\mathrm{ref}}}$ denote the reference policy, which in practice is the frozen base model (DeepMedix). G is the number of responses sampled per question in each iteration. For each question q, GRPO samples a group of outputs $\{o_1, o_2, \cdots, o_G\}$ from the old policy model $\pi_{\theta_{\mathrm{old}}}$. The policy model π_θ is optimized by maximizing the objective:

$$\mathcal{J}_{GRPO}(\theta) = \mathbb{E}[q \sim P(Q), \{o_i\}_{i=1}^{G} \sim \pi_{\theta_{old}}(O|q)]$$
$$\frac{1}{G}\sum_{i=1}^{G}\frac{1}{|o_i|}\sum_{t=1}^{|o_i|}\left\{\min\left[\frac{\pi_\theta(o_{i,t}|q,o_{i,<t})}{\pi_{\theta_{old}}(o_{i,t}|q,o_{i,<t})}\hat{A}_{i,t}, \mathrm{clip}\left(\frac{\pi_\theta(o_{i,t}|q,o_{i,<t})}{\pi_{\theta_{old}}(o_{i,t}|q,o_{i,<t})}, 1-\epsilon, 1+\epsilon\right)\hat{A}_{i,t}\right] - \beta\mathbb{D}_{KL}\left[\pi_\theta||\pi_{ref}\right]\right\}. \tag{2}$$

ϵ and β are hyper-parameters. The KL divergence [52] term serves as a regularization for the policy update, preventing π_θ from deviating too far from the reference model $\pi_{\theta_{old}}$. It is estimated using the following unbiased estimator:

$$\mathbb{D}_{KL}\left[\pi_\theta||\pi_{ref}\right] = \frac{\pi_{ref}(o_{i,t}|q,o_{i,<t})}{\pi_\theta(o_{i,t}|q,o_{i,<t})} - \log\frac{\pi_{ref}(o_{i,t}|q,o_{i,<t})}{\pi_\theta(o_{i,t}|q,o_{i,<t})} - 1, \tag{3}$$

[1] https://openai.com/index/gpt-4-1/

where π_{ref} is the reference model which is usually the initial fine-tuned DeepMedix model. β is the coefficient of the KL penalty. $\hat{A}_{i,t}$ represents the advantage computed using relative rewards among outputs within each group. Suppose a group of outputs $\{o_1, o_2, \cdots, o_G\}$ has reward $\mathbf{r} = \{r_1, r_2, \cdots, r_G\}$, there is $\hat{A}_{i,t} = \frac{r_i - \text{mean}(\mathbf{r})}{\text{std}(\mathbf{r})}$. For each output o_i and its ground label l_i, we set its reward r_i based on three distinct perspectives, i.e., answer score, image coordinate score, and format score. The answer score directly reflects the alignment degree between the generated answer and the ground truth, given by:

$$r_{ans,i} = 1.5 * \begin{cases} \mathbb{I}(o_i = l_i), & \text{closed-ended questions} \\ \text{F1}(o_i, l_i), & \text{multi-object questions} \\ 1/3[\text{BLEU}_1(o_i, l_i) + \text{BLEU}_4(o_i, l_i) + \text{ROUGE} - \text{L}(o_i, l_i)], & \text{otherwise.} \end{cases} \tag{4}$$

Image coordinate scores focus the model's awareness on specific local grounded regions within CXRs, given by:

$$r_{coo,i} = \max\big(\text{N}_{coo}(o_i) * 0.05 + \phi(o_i), 0.15\big). \tag{5}$$

N_{coo} function counts the number of coordinates presented in the reasoning process. ϕ is the deviation control parameter, and we set it to -0.2, which means that if the coordinate is beyond the range of the X-ray image then we set a penalty. The format score indicates if the model response followed the predefined format, i.e., the thinking process in the "<think>...</think>" tag and the final result in "\boxed{}" tag, given by:

$$r_{fom,i} = \begin{cases} 1.0 & \text{conforms to format} \\ 0.0 & \text{otherwise.} \end{cases} \tag{6}$$

Finallly, the final reward is formally as: $r_i = (1 - \lambda) r_{ans,i} + \lambda r_{fom,i} + r_{coo,i}$. The λ is set to 0.1 as the default.

Report Arena

To give a comprehensive evaluation of cutting-edge open-sourced vision-language FMs, automated NLG metrics (BLEU, METEOR, and ROUGE-L) and fact metrics (F1-RadGraph and F1-CheXbert) are utilized on report generation tasks. In the VQA tasks, we utilize the overall accuracy covering both exact match accuracy of closed-ended questions and F1 scores for *multi-object* questions that need to predict a set of abnormalities, positions or attributes. Beyond these automated metrics for evaluation, inspired by Chatbot Arena [35, 53], we implement an LLM-as-judge evaluation framework, namely Report Arena to comparatively assess paired outputs from competing models on report generation tasks. Suppose there are totally M models, $m_1, m_2 \in [\text{M}]$ are the indices of the models. We define $A_t = (m_1, m_2)$ as the model pair at time t, and the response from LLM is $H_t \in \{0, 1\}$, indicating whether model m_1 is better than m_2 for a specific report generation given a CXR image. In the current stage t, the probability $P_t(a)$ for sampling model pair a for evaluation is given by:

$$P_t(a) \propto \sqrt{\frac{\hat{\sum}_{t,a,a}}{|\{t : A_t = a\}|}} - \sqrt{\frac{\hat{\sum}_{t,a,a}}{|\{t : A_t = a\}| + 1}}, \tag{7}$$

where $\hat{\sum}_t$ is the estimated covariance matrix. After the sampling and judging process, the Bradley-Terry [54] model with the logistic form is implemented to calculate scores for all models:

$$\hat{s} = \arg\min_{\xi} \sum_{t=1}^{T} \frac{1}{P(A_t)} \text{CE}\big(H_t, \frac{1}{1 + e^{\xi_{A_{t,2}} - \xi_{A_{t,1}}}}\big), \tag{8}$$

where ξ is a M-dimensional vector to represent model scores and CE is the binary cross-entropy loss. Based on the learned ranking scores, we normalized them to the [0,1] range using max-absolute scaling. We totally sample 6K pairs for evaluation.

Expert Annotation

For the final reasoning processing annotation, we design five metrics covering three progressive levels:

(1) Reasoning step. Reflecting the detail of each reasoning step of reasoning processing, metric *Relevance* and *Correctness* are utilized. The former indicates whether the content described in the

specific step is relevant to the correct answer, while the latter denotes whether the content described in the specific step truly reflects the CXR content, including specific local regions.

(2) The whole reasoning process of models. Metric *Completeness* is utilized, indicating whether the reasoning process is complete, i.e., for obtaining the correct answer, are all the reasoning process descriptions provided by the model sufficient?

(3) Reasoning preference for samples. Given the sample and the generated reasoning process by models, we need to judge which model is better. Metric *Grounded Preference* and *Overall Preference* are introduced. The former evaluates the fine-grained image description of the overall reasoning process and determines which model is better, covering whether there are fine-grained descriptions, their correctness, and their correlation regarding the correct answer. The latter evaluates the professionalism of the overall reasoning process and the extent to which the correct answer can be obtained through reasoning.

For the annotation, we randomly sampled 210 samples and their reasoning processing generated by DeepMedix-R1 and Qwen2.5-VL-7B (think) from XrayBench (as other medical-specific models have no ability to generate the reasoning processing for the answer). Four expert CXR physicians were divided into two groups for annotation, with each group responsible for evaluating all samples.

Data availability

The MIMIC-CXR dataset is publicly accessible on PhysioNet (https://physionet.org/content/mimic-cxr-jpg/2.1.0/). The OpenI dataset can be downloaded from Kaggle (https://www.kaggle.com/datasets/raddar/chest-xrays-indiana-university). The MS-CXR dataset is available on PhysioNet (https://physionet.org/content/ms-cxr/1.1.0/). For visual question-answering (VQA) tasks, the Ext-VQA and CXR-VQA datasets are also available on PhysioNet (https://physionet.org/content/mimic-ext-mimic-cxr-vqa/1.0.0/, https://physionet.org/content/medical-cxr-vqa-dataset/1.0.0/) The XrayBench is available via Huggingface (https://huggingface.co/datasets/Qika/xraybench).

Code availability

The model is trained with LLaMA-Factory (https://github.com/hiyouga/LLaMA-Factory) and EasyR1 (https://github.com/hiyouga/EasyR1). The source codes are available online at https://github.com/DeepReasoning/DeepMedix-R1. The final DeepMedix-R1 is available online at https://huggingface.co/Qika/DeepMedix-R1.

References

[1] Wayne Xin Zhao, Kun Zhou, Junyi Li, Tianyi Tang, Xiaolei Wang, Yupeng Hou, Yingqian Min, Beichen Zhang, Junjie Zhang, Zican Dong, et al. A survey of large language models. *arXiv preprint arXiv:2303.18223*, 2023.

[2] Shukang Yin, Chaoyou Fu, Sirui Zhao, Ke Li, Xing Sun, Tong Xu, and Enhong Chen. A survey on multimodal large language models. *National Science Review*, 11(12):nwae403, 2024.

[3] Nanyi Fei, Zhiwu Lu, Yizhao Gao, Guoxing Yang, Yuqi Huo, Jingyuan Wen, Haoyu Lu, Ruihua Song, Xin Gao, Tao Xiang, et al. Towards artificial general intelligence via a multimodal foundation model. *Nature Communications*, 13(1):3094, 2022.

[4] Michael Moor, Oishi Banerjee, Zahra Shakeri Hossein Abad, Harlan M Krumholz, Jure Leskovec, Eric J Topol, and Pranav Rajpurkar. Foundation models for generalist medical artificial intelligence. *Nature*, 616(7956):259–265, 2023.

[5] Kai Zhang, Rong Zhou, Eashan Adhikarla, Zhiling Yan, Yixin Liu, Jun Yu, Zhengliang Liu, Xun Chen, Brian D Davison, Hui Ren, et al. A generalist vision–language foundation model for diverse biomedical tasks. *Nature Medicine*, pages 1–13, 2024.

[6] Angelina Wang, Jamie Morgenstern, and John P Dickerson. Large language models that replace human participants can harmfully misportray and flatten identity groups. *Nature Machine Intelligence*, pages 1–12, 2025.

[7] Jiankai Sun, Chuanyang Zheng, Enze Xie, Zhengying Liu, Ruihang Chu, Jianing Qiu, Jiaqi Xu, Mingyu Ding, Hongyang Li, Mengzhe Geng, et al. A survey of reasoning with foundation models: Concepts, methodologies, and outlook. *ACM Computing Surveys*, 57(11):1–43, 2025.

[8] Muhammad Awais, Muzammal Naseer, Salman Khan, Rao Muhammad Anwer, Hisham Cholakkal, Mubarak Shah, Ming-Hsuan Yang, and Fahad Shahbaz Khan. Foundation models defining a new era in vision: a survey and outlook. *IEEE Transactions on Pattern Analysis and Machine Intelligence*, 2025.

[9] Arun James Thirunavukarasu, Darren Shu Jeng Ting, Kabilan Elangovan, Laura Gutierrez, Ting Fang Tan, and Daniel Shu Wei Ting. Large language models in medicine. *Nature medicine*, 29(8):1930–1940, 2023.

[10] Qika Lin, Yifan Zhu, Xin Mei, Ling Huang, Jingying Ma, Kai He, Zhen Peng, Erik Cambria, and Mengling Feng. Has multimodal learning delivered universal intelligence in healthcare? A comprehensive survey. *Information Fusion*, 116:102795, 2025.

[11] Karan Singhal, Tao Tu, Juraj Gottweis, Rory Sayres, Ellery Wulczyn, Mohamed Amin, Le Hou, Kevin Clark, Stephen R Pfohl, Heather Cole-Lewis, et al. Toward expert-level medical question answering with large language models. *Nature Medicine*, 31(3):943–950, 2025.

[12] Kai He, Rui Mao, Qika Lin, Yucheng Ruan, Xiang Lan, Mengling Feng, and Erik Cambria. A survey of large language models for healthcare: from data, technology, and applications to accountability and ethics. *Information Fusion*, 118:102963, 2025.

[13] Wasif Khan, Seowung Leem, Kyle B See, Joshua K Wong, Shaoting Zhang, and Ruogu Fang. A comprehensive survey of foundation models in medicine. *IEEE Reviews in Biomedical Engineering*, 2025.

[14] Chunyuan Li, Cliff Wong, Sheng Zhang, Naoto Usuyama, Haotian Liu, Jianwei Yang, Tristan Naumann, Hoifung Poon, and Jianfeng Gao. Llava-med: training a large language-and-vision assistant for biomedicine in one day. In *Proceedings of the 37th International Conference on Neural Information Processing Systems*, pages 28541–28564, 2023.

[15] Zeyu Gao, Kai He, Weiheng Su, Ines P Machado, William McGough, Mercedes Jimenez-Linan, Brian Rous, Chunbao Wang, Chengzu Li, Xiaobo Pang, et al. Alpaca: Adapting llama for pathology context analysis to enable slide-level question answering. *medRxiv*, pages 2025–04, 2025.

[16] Juan Manuel Zambrano Chaves, Shih-Cheng Huang, Yanbo Xu, Hanwen Xu, Naoto Usuyama, Sheng Zhang, Fei Wang, Yujia Xie, Mahmoud Khademi, Ziyi Yang, et al. A clinically accessible small multimodal radiology model and evaluation metric for chest x-ray findings. *Nature Communications*, 16(1):3108, 2025.

[17] Munib Mesinovic, Peter Watkinson, and Tingting Zhu. Explainability in the age of large language models for healthcare. *Communications Engineering*, 4(1):128, 2025.

[18] Valentin Liévin, Christoffer Egeberg Hother, Andreas Geert Motzfeldt, and Ole Winther. Can large language models reason about medical questions? *Patterns*, 5(3), 2024.

[19] Yuxiang Lai, Jike Zhong, Ming Li, Shitian Zhao, and Xiaofeng Yang. Med-r1: Reinforcement learning for generalizable medical reasoning in vision-language models. *arXiv preprint arXiv:2503.13939*, 2025.

[20] Shruthi Bannur, Kenza Bouzid, Daniel C Castro, Anton Schwaighofer, Anja Thieme, Sam Bond-Taylor, Maximilian Ilse, Fernando Pérez-García, Valentina Salvatelli, Harshita Sharma, et al. Maira-2: Grounded radiology report generation. *arXiv preprint arXiv:2406.04449*, 2024.

[21] Sergio Sanchez Santiesteban, Muhammad Awais, Yi-Zhe Song, and Josef Kittler. Enhancing radiology report generation: the impact of locally grounded vision and language training. In *35th British Machine Vision Conference. Glasgow, UK: BMVA*, 2024.

[22] Zhixuan Chen, Yequan Bie, Haibo Jin, and Hao Chen. Large language model with region-guided referring and grounding for ct report generation. *IEEE Transactions on Medical Imaging*, 2025.

[23] Kaiming Dong, Yuxiao Cheng, Kunlun He, and Jinli Suo. A generative model uses healthy and diseased image pairs for pixel-level chest x-ray pathology localization. *Nature Biomedical Engineering*, pages 1–13, 2025.

[24] Daniel Coelho de Castro, Aurelia Bustos, Shruthi Bannur, Stephanie L Hyland, Kenza Bouzid, Maria Teodora Wetscherek, Maria Dolores Sánchez-Valverde, Lara Jaques-Pérez, Lourdes Pérez-Rodríguez, Kenji Takeda, et al. Padchest-gr: A bilingual chest x-ray dataset for grounded radiology report generation. *NEJM AI*, 2(7):AIdbp2401120, 2025.

[25] Yupeng Chang, Xu Wang, Jindong Wang, Yuan Wu, Linyi Yang, Kaijie Zhu, Hao Chen, Xiaoyuan Yi, Cunxiang Wang, Yidong Wang, et al. A survey on evaluation of large language models. *ACM Transactions on Intelligent Systems and Technology*, 15(3):1–45, 2024.

[26] Kishore Papineni, Salim Roukos, Todd Ward, and Wei-Jing Zhu. Bleu: a method for automatic evaluation of machine translation. In *Proceedings of the 40th annual meeting of the Association for Computational Linguistics*, pages 311–318, 2002.

[27] Alon Lavie and Abhaya Agarwal. METEOR: an automatic metric for MT evaluation with high levels of correlation with human judgments. In Chris Callison-Burch, Philipp Koehn, Cameron S. Fordyce, and Christof Monz, editors, *Proceedings of the Second Workshop on Statistical Machine Translation*, pages 228–231, 2007.

[28] Chin-Yew Lin. Rouge: A package for automatic evaluation of summaries. In *Text Summarization Branches Out*, pages 74–81, 2004.

[29] Qwen Team. Qwen2.5-vl, January 2025. URL `https://qwenlm.github.io/blog/qwen2.5-vl/`.

[30] Zhihong Shao, Peiyi Wang, Qihao Zhu, Runxin Xu, Junxiao Song, Xiao Bi, Haowei Zhang, Mingchuan Zhang, YK Li, Y Wu, et al. Deepseekmath: Pushing the limits of mathematical reasoning in open language models. *arXiv preprint arXiv:2402.03300*, 2024.

[31] Lai Wei, Yuting Li, Kaipeng Zheng, Chen Wang, Yue Wang, Linghe Kong, Lichao Sun, and Weiran Huang. Advancing multimodal reasoning via reinforcement learning with cold start. *arXiv preprint arXiv:2505.22334*, 2025.

[32] Saahil Jain, Ashwin Agrawal, Adriel Saporta, Steven Q. H. Truong, Du Nguyen Duong, Tan Bui, Pierre J. Chambon, Yuhao Zhang, Matthew P. Lungren, Andrew Y. Ng, Curtis P. Langlotz, and Pranav Rajpurkar. Radgraph: Extracting clinical entities and relations from radiology reports. In *Proceedings of the Neural Information Processing Systems Track on Datasets and Benchmarks*, 2021.

[33] Akshay Smit, Saahil Jain, Pranav Rajpurkar, Anuj Pareek, Andrew Y Ng, and Matthew Lungren. Combining automatic labelers and expert annotations for accurate radiology report labeling using bert. In *Proceedings of the 2020 Conference on Empirical Methods in Natural Language Processing (EMNLP)*, pages 1500–1519, 2020.

[34] Google. Medgemma hugging face. `https://huggingface.co/collections/google/medgemma-release-680aade845f90bec6a3f60c4`, 2025. Accessed: 2025-06-10.

[35] Wei-Lin Chiang, Lianmin Zheng, Ying Sheng, Anastasios Nikolas Angelopoulos, Tianle Li, Dacheng Li, Banghua Zhu, Hao Zhang, Michael Jordan, Joseph E Gonzalez, et al. Chatbot arena: An open platform for evaluating llms by human preference. In *Forty-first International Conference on Machine Learning*, 2024.

[36] Haoyu Lu, Wen Liu, Bo Zhang, Bingxuan Wang, Kai Dong, Bo Liu, Jingxiang Sun, Tongzheng Ren, Zhuoshu Li, Hao Yang, et al. Deepseek-vl: towards real-world vision-language understanding. *arXiv preprint arXiv:2403.05525*, 2024.

[37] Junying Chen, Ruyi Ouyang, Anningzhe Gao, Shunian Chen, Guiming Hardy Chen, Xidong Wang, Ruifei Zhang, Zhenyang Cai, Ke Ji, Guangjun Yu, Xiang Wan, and Benyou Wang. Huatuogpt-vision, towards injecting medical visual knowledge into multimodal llms at scale, 2024. URL `https://arxiv.org/abs/2406.19280`.

[38] Zhihong Chen, Maya Varma, Jean-Benoit Delbrouck, Magdalini Paschali, Louis Blankemeier, Dave Van Veen, Jeya Maria Jose Valanarasu, Alaa Youssef, Joseph Paul Cohen, Eduardo Pontes Reis, et al. Chexagent: Towards a foundation model for chest x-ray interpretation. *arXiv preprint arXiv:2401.12208*, 2024.

[39] Alistair EW Johnson, Tom J Pollard, Seth J Berkowitz, Nathaniel R Greenbaum, Matthew P Lungren, Chih-ying Deng, Roger G Mark, and Steven Horng. Mimic-cxr, a de-identified publicly available database of chest radiographs with free-text reports. *Scientific data*, 6(1):317, 2019.

[40] Dina Demner-Fushman, Sameer Antani, Matthew Simpson, and George R Thoma. Design and development of a multimodal biomedical information retrieval system. *Journal of Computing Science and Engineering*, 6(2):168–177, 2012.

[41] Seongsu Bae, Daeun Kyung, Jaehee Ryu, Eunbyeol Cho, Gyubok Lee, Sunjun Kweon, Jungwoo Oh, Lei Ji, Eric Chang, Tackeun Kim, et al. Mimic-ext-mimic-cxr-vqa: A complex, diverse, and large-scale visual question answering dataset for chest x-ray images, 2024.

[42] Xinyue Hu, Lin Gu, Kazuma Kobayashi, Liangchen Liu, Mengliang Zhang, Tatsuya Harada, Ronald Summers, and Yingying Zhu. Medical-cxr-vqa dataset: A large-scale llm-enhanced medical dataset for visual question answering on chest x-ray images, 2025.

[43] Sebastian Farquhar, Jannik Kossen, Lorenz Kuhn, and Yarin Gal. Detecting hallucinations in large language models using semantic entropy. *Nature*, 630(8017):625–630, 2024.

[44] Xiaoman Zhang, Chaoyi Wu, Ya Zhang, Weidi Xie, and Yanfeng Wang. Knowledge-enhanced visual-language pre-training on chest radiology images. *Nature Communications*, 14(1):4542, 2023.

[45] Junwei Yang, Hanwen Xu, Srbuhi Mirzoyan, Tong Chen, Zixuan Liu, Zequn Liu, Wei Ju, Luchen Liu, Zhiping Xiao, Ming Zhang, et al. Poisoning medical knowledge using large language models. *Nature Machine Intelligence*, 6(10):1156–1168, 2024.

[46] Fangzhi Xu, Zhiyong Wu, Qiushi Sun, Siyu Ren, Fei Yuan, Shuai Yuan, Qika Lin, Yu Qiao, and Jun Liu. Symbol-llm: Towards foundational symbol-centric interface for large language models. In *ACL*, pages 13091–13116, 2024.

[47] Jian Zhang, Bifan Wei, Shihao Qi, Jun Liu, and Qika Lin. Gkg-llm: A unified framework for generalized knowledge graph construction. *arXiv preprint arXiv:2503.11227*, 2025.

[48] Kai He, Yucheng Huang, Wenqing Wang, Delong Ran, Dongming Sheng, Junxuan Huang, Qika Lin, Jiaxing Xu, Wenqiang Liu, and Mengling Feng. Crab: A novel configurable role-playing llm with assessing benchmark. In *ACL*, pages 15030–15052, 2025.

[49] Zhihe Yang, Xufang Luo, Dongqi Han, Yunjian Xu, and Dongsheng Li. Mitigating hallucinations in large vision-language models via dpo: On-policy data hold the key. In *Proceedings of the Computer Vision and Pattern Recognition Conference*, pages 10610–10620, 2025.

[50] Alice Heiman, Xiaoman Zhang, Emma Chen, Sung Eun Kim, and Pranav Rajpurkar. Factchexcker: Mitigating measurement hallucinations in chest x-ray report generation models. In *Proceedings of the Computer Vision and Pattern Recognition Conference*, pages 30787–30796, 2025.

[51] Liang Chen, Zekun Wang, Shuhuai Ren, Lei Li, Haozhe Zhao, Yunshui Li, Zefan Cai, Hongcheng Guo, Lei Zhang, Yizhe Xiong, et al. Next token prediction towards multimodal intelligence: A comprehensive survey. *arXiv preprint arXiv:2412.18619*, 2024.

[52] Solomon Kullback and Richard A Leibler. On information and sufficiency. *The annals of mathematical statistics*, 22(1):79–86, 1951.

[53] Kanzhi Cheng, Wenpo Song, Jiaxin Fan, Zheng Ma, Qiushi Sun, Fangzhi Xu, Chenyang Yan, Nuo Chen, Jianbing Zhang, and Jiajun Chen. Caparena: Benchmarking and analyzing detailed image captioning in the llm era. *arXiv preprint arXiv:2503.12329*, 2025.

[54] Ralph Allan Bradley and Milton E Terry. Rank analysis of incomplete block designs: I. the method of paired comparisons. *Biometrika*, 39(3/4):324–345, 1952.